Journal of Statistical Physics, Vol. 94, Nos. 1/2, 1999

Correlation Functions by Cluster Variation Method for Ising Model with NN, NNN, and Plaquette Interactions

E. N. M. Cirillo,[1] G. Gonnella,[2] M. Troccoli,[2] and A. Maritan[3]

Received May 12, 1998

We consider a procedure for calculating the pair correlation function in the context of cluster variation methods (CVM). As specific cases, we study the pair correlation function in the paramagnetic phase of the Ising model with nearest neighbors, next to nearest neighbors, and plaquette interactions in two and three dimensions. In presence of competing interactions, the so-called disorder line separates in the paramagnetic phase a region where the correlation function has the usual exponential behavior from a region where the correlation has an oscillating, exponentially damped behavior. In two dimensions, using the plaquette as the maximal cluster of the CVM approximation, we calculate the phase diagram and the disorder line for a case where a comparison is possible with known results for the eight-vertex model. In three dimensions, in the CVM cube approximation, we calculate the phase diagram and the disorder line in some cases of particular interest. The relevance of our results for experimental systems like mixtures of oil, water, and surfactant is also discussed.

KEY WORDS: Ising models; CVM; correlation functions; disorder line.

I. INTRODUCTION

Statistical systems are exactly solvable only in the simplest cases and often in unphysical spatial dimensions. In three dimensions, in particular, solutions of common statistical models like the Ising model are not known. On the other hand, numerical simulations sometimes are not a very efficient

[1] Université Paris Sud, 91405 Orsay Cedex, France; e-mail: Emilio.Cirillo@math.u-psud.fr.
[2] Dipartimento di Fisica dell'Università di Bari and Istituto Nazionale per la Fisica della Materia, 70126 Bari, Italy; e-mail: gonnella@ba.infn.it, troccoli@bari.infn.it.
[3] S.I.S.S.A.—International School for Advanced Studies and Istituto Nazionale per la Fisica della Materia, 34014 Trieste, Italy.

0022-4715/99/0100-0067$16.00/0

tool for studying systems with complex phase diagrams where an analytical control of the phase behavior of the system would be very helpful. If one is not interested in the critical behavior of the system, a very useful generalization of mean field methods for studying the phase diagram of spin systems is given by the cluster variation method (CVM).[1–3] This method generally gives a very accurate description of the phase diagram that can be appreciated when a comparison is possible with exact or Monte Carlo results?[4] It has been extensively used for the calculation of equilibrium thermodynamics properties of spin models.

The CVM is based on the application of the variational principle of the statistical mechanics with the simplification that the density matrix of the system is factorized over clusters inside which the system is treated exactly. The size of these cluster, sometimes called "maximal clusters," depends on the accuracy requested and on the necessity of including all the interaction of the system and of reproducing the structure of the ground-states. Correlation functions have been calculated in the framework of CVM approximation only in few simple cases. Some properties of the pair correlation function of the two-dimensional Ising model have been studied in the pair (Bethe) and plaquette approximation levels of the CVM.[5] The CVM has been also applied to the study of the correlation function in the disordered phase of the two-dimensional ANNNI (Axial Next Nearest Neighbors Ising) model.[6]

In this paper we present a procedure for the calculation of correlation functions that can be generally applied to any choice of maximal cluster in the CVM scheme. It can be also implemented in numerical calculations together with the Natural Iteration Method[7] which is a numerical minimization procedure very convenient for calculating the maximal cluster density matrix in the most complex cases. In particular we apply our procedure to study the behavior of the pair correlation functions in the paramagnetic phase of the Ising model with nearest neighbors (NN), next-to-the-nearest neighbors (NNN), and plaquette (P) interactions in two and three dimensions. In three dimensions, the phase diagram of this model can be correctly studied by implementing the CVM cube approximation with 8 independent site magnetizations in order to take into account the complex ground-state structure. Our goal will be to calculate the pair correlation function in the same approximation used for the phase diagram.

The model with NN, NNN, and P interactions has the same hamiltonian of the symmetric two-dimensional eight-vertex models.[8] In three-dimensions this model is interesting also because it constitutes a realization of interacting random surfaces on a lattice.[9, 10] Indeed, the Peierls interfaces between domains of different sign can be interpreted as an ensemble of interacting surfaces with a Boltzmann weight depending on the area,

the mean curvature and the length of the intersection lines between the surfaces.[10] It has been shown[11, 12] that the phase diagram of this model, studied in mean field approximation, can well describe the phase diagram of experimental systems like fluid mixtures of water, oil, and surfactant or other complex fluids. Recently, the model with NN, NNN, and P interactions has been also put in relation with string theory and in particular with a discretized string model (the so-called gonihedric model) characterized by a zero energy cost for the area of surfaces.[13] The CVM cube approximation has been applied to the study of the phase diagram of the model with NN, NNN, and P interactions in the parameter region corresponding to the gonihedric model.[14]

A question of particular interest in the phase diagram of models with competing interactions is the behavior of the pair correlation function in the paramagnetic phase. Here, generally, the so called "disorder line" separates a region where the pair correlation has the usual exponentially damped behavior from a region where the correlation develops an oscillatory exponentially damped behavior.[15] In the case of the three-dimensional model with NN, NNN, P interactions, this latter region can be identified with the microemulsion phase of surfactant systems which is a disordered phase but with an ordered structure on short length-scales.[16] Therefore, in this model, the possibility of calculating the correlation functions in the same CVM approximation used for the phase diagram is interesting also for some physical applications.

The plan of the paper is the following. In Section II we briefly summarize the CVM procedure and discuss how correlation functions can be calculated. In Section III we consider the bidimensional eight-vertex model. We calculate the disorder line and compare our results with other results existing in literature. In Section IV we will carry out the calculation of the correlation functions in the three-dimensional case and study the disorder line in two cases of particular physical interest. Some conclusions will follow.

II. CVM AND CORRELATION FUNCTIONS

In this section we first briefly describe the CVM approximation. We refer to the papers of refs. 2 for further details. Then we will discuss how the pair correlation functions can be evaluated starting from the CVM free energy.

Suppose to have a spin hamiltonian defined on a given lattice as

$$-\beta\mathscr{H}(\sigma)=\sum_{\alpha\in\mathscr{I}}J_\alpha\sigma_\alpha \tag{1}$$

where β is the inverse of the temperature, J_α is the interaction parameter for the cluster α and σ_α is the product of spins σ_i on the sites $i \in \alpha$. The first step of the CVM procedure is to choose a set of maximal clusters $\mathscr{M}$ in which the system is treated exactly such that each cluster $\alpha \in \mathscr{I}$ is included in one maximal cluster $M \in \mathscr{M}$. Then the CVM approximated free energy of the system can be expressed[2] as the minimum of

$$\beta \mathscr{F} = -\sum_{\alpha \in \mathscr{I}} J_\alpha \xi_\alpha + \sum_{\alpha \subseteq M \in \mathscr{M}} a_\alpha \operatorname{Tr} \rho_\alpha \ln \rho_\alpha \tag{2}$$

Here the first sum is the internal energy of the system with the ξ_α being variational parameters representing the expectation value of the multisite product of spins σ_α. The second term in the r.h.s of (2) is the entropy of the system and is a sum over all the clusters which are possible subclusters of the maximal clusters. The set of coefficients a_α depends on the lattice structure and on the choice of the maximal cluster; they can be easily found applying the Eqs. (16′) in the paper by An.[2] The trace Tr is the sum over the allowed configurations and ρ_α is the density matrix for the cluster α. In the case of Ising spins $\sigma_i = \pm 1$ one can write

$$\rho_\alpha = 2^{-n_\alpha} \left[1 + \sum_{\beta \subseteq \alpha} \sigma_\beta \xi_\beta \right] \tag{3}$$

where n_α is the number of the sites in the cluster α, the sum extends over all the subclusters β of the cluster α, and $\sigma_\beta = \prod_{i \in \beta} \sigma_i$. A consequence of Eq. (3) is that $\xi_\beta = \operatorname{Tr} \sigma_\beta \rho_\beta$ for a cluster $\beta \subseteq \alpha$. The parameters ξ_α have to verify the minimization conditions

$$0 = \frac{\partial \mathscr{F}}{\partial \xi_\alpha} \tag{4}$$

In order to study the pair correlation function for a group of spins σ_γ, it is convenient to introduce a local external field in the starting hamiltonian coupled to all clusters of the same type of γ. For one of these clusters the equilibrium condition becomes

$$h_\gamma = \frac{\partial \mathscr{F}}{\partial \xi_\gamma} \tag{5}$$

Therefore the connected pair correlation function is given by

$$\langle \sigma_{\gamma_0} \sigma_{\gamma_{\vec{r}}} \rangle_c = \frac{\partial^2 \mathscr{F}}{\partial h_{\gamma_0} \partial h_{\gamma_{\vec{r}}}} = \frac{\partial \xi_{\gamma_0}}{\partial h_{\gamma_{\vec{r}}}} \tag{6}$$

where we have used the linear response theorem and the equilibrium conditions (4). Now, the free energy $\mathscr{F}(J_\alpha, h_\gamma)$ can be considered formally as a function of the independent variables ξ_γ instead of the h_γ. Therefore the last term of the above equation can be evaluated through its inverse matrix that can be calculated by differentiating (5) with respect to $\xi_{\gamma_{\bar{r}}}$:

$$\frac{\partial h_{\gamma_0}}{\partial \xi_{\gamma_{\bar{r}}}} = \frac{\partial^2 \mathscr{F}}{\partial \xi_{\gamma_{\bar{0}}} \partial \xi_{\gamma_{\bar{r}}}} \equiv \mathscr{A}_{\gamma_0, \gamma_{\bar{r}}} \tag{7}$$

Once that the above matrix is obtained, its Fourier transform can be simply inverted and will give the requested correlation function in Fourier space. However, except that in the simplest cases, writing the matrix $\mathscr{A}_{\gamma_0, \gamma_{\bar{r}}}$ can be a complicate task from a computational point of view and requires some further considerations that we present here in a general way and that will become more transparent when applied to specific examples in the next sections.

In the matrix $\mathscr{A}_{\gamma_0, \gamma_{\bar{r}}}$ there appear generally derivatives like $\partial \xi_\alpha / \partial \xi_\gamma$ (see, e.g., Eqs. (15, 16)) where γ is a cluster of different type of α. The evaluation of these derivatives can be performed by differentiating the state equations for ξ_α with respect to ξ_γ. This procedure will give a system of linear equations

$$\frac{\partial^2 \mathscr{F}}{\partial \xi_\alpha \partial \xi_\gamma} = 0 \tag{8}$$

in the variables $\partial \xi_\alpha / \partial \xi_\gamma$. Some of the equations (8) are homogeneous. More specifically these situations may occur: (i) the cluster α belongs only to one maximal cluster. In such a case the equation (8) is homogeneous or not, depending if γ is external or not to that maximal cluster. (ii) The cluster α belongs to more than one maximal cluster and γ is external to the maximal clusters with α in common. In such a case the equation (8) is homogeneous. (iii) The cluster α belongs to more than one maximal cluster and γ belongs to one of the maximal clusters with α in common. In this case the equation is generally not homogeneous. It can be shown that a solution of the system (8) can be obtained by setting equal to zero all the terms $\partial \xi_\alpha / \partial \xi_\gamma$ appearing in homogeneous equations. This procedure will be more clear and it will be shown in explicit cases in the next two sections.

Finally we observe that a great simplification occurs when we want to calculate the correlation function in the paramagnetic phase of a system with only even interactions. In this case only the derivatives $\partial \xi_\alpha / \partial \xi_\gamma$, where α and γ have both an odd (or even) number of sites, are different from zero.

III. PAIR CORRELATION IN THE 8-VERTEX MODEL

In the following of the paper our principal aim will be to calculate the two-spin correlation function and the disorder line of the model defined by the hamiltonian

$$-\beta\mathscr{H} = J_1 \sum_{\langle x,\, y\rangle} \sigma_x\sigma_y + J_2 \sum_{\langle\langle x,\, y\rangle\rangle} \sigma_x\sigma_y + J_3 \sum_{\substack{x\\ y\square z\\ w}} \sigma_x\sigma_w\sigma_z\sigma_y \tag{9}$$

where β is the inverse of the temperature and the σ_x are Ising variables defined on the sites of a cubic lattice. The three sums respectively refer to nearest, next-to-the nearest neighbors and plaquettes of the lattice. In this section we consider the CVM plaquette approximation of this hamiltonian on a square lattice and we use it to calculate the phase diagram, the correlation function in the disordered phase and the disorder line in the case $J_3 = 0$. In the following section we will consider the three-dimensional case.

3.1. The Plaquette Approximation and the Phase Diagram

The natural choice for studying the phase diagram of the model (9) in two dimensions is the CVM approximation level where the maximal cluster with independent density matrix is the plaquette cell of the square lattice. When a magnetic-field term is added to (9), the CVM free-energy density functional $\mathscr{F}$ to be minimized is given by

$$\begin{aligned}\beta\mathscr{F} = &-J_1 \sum_{\langle xy\rangle} \mathrm{Tr}(\sigma_x\sigma_y\rho_{\langle xy\rangle}) - J_2 \sum_{\langle\langle xy\rangle\rangle} \mathrm{Tr}(\sigma_x\sigma_y\rho_{\langle\langle xy\rangle\rangle})\\ &- J_3 \sum_{\substack{x\\ y\square z\\ w}} \mathrm{Tr}(\sigma_x\sigma_y\sigma_w\sigma_z\rho_{\substack{x\\ y\square z\\ w}}) - \beta\sum_x h_x\,\mathrm{Tr}(\sigma_x\rho_x)\\ &+ \sum_{\substack{x\\ y\square z\\ w}} \mathrm{Tr}\,\mathscr{L}(\rho_{\substack{x\\ y\square z\\ w}}) - \sum_{\langle xy\rangle} \mathrm{Tr}\,\mathscr{L}(\rho_{\langle xy\rangle}) + \sum_x \mathrm{Tr}\,\mathscr{L}(\rho_x)\end{aligned} \tag{10}$$

where the spins σ_x in the argument of the traces are the spins in the cluster one is considering, $\mathscr{L}(a) = a\log a$ for a real number a and ρ_α is the density matrix related to the cluster of a given type α of the lattice; in the following we need also the matrix $\rho_{[xyz]}$ where $[xyz]$ denotes a three site corner cluster. The density matrix $\rho_\square$ is subjected to the constraint $\mathrm{Tr}\,\rho_\square = 1$ and the smaller cluster density matrices are obtained by partial traces of $\rho_\square$. Notice that we have not assumed any *a priori* symmetry property for our density matrices; this implies that all possible states with different magnetic order in a single plaquette can be studied by this approximation.

The plaquette density matrix $\rho_{\square}$ can be calculated by minimizing the free energy (10) via the natural iteration equations;[7] then, after partial traces, one can work out the phase diagram of the system. In Fig. 1 the portion of the phase diagram with $J_3 = 0$ is shown. The line separating the ferromagnetic and the paramagnetic phases is critical, while on the line separating the paramagnetic and the lamellar phase—sometimes called Super AntiFerromagnetic (SAF) phase—there is a tricritical point at $J_1 = 0.405 \pm 0.005$, $J_2 = -0.4045 \pm 0.0015$. The existence of a first order phase transition between the paramagnetic and the lamellar phase is also confirmed by other authors[18, 19] that have used the plaquette CVM approximation to study the phase diagram of the 8-vertex model. Our results for the location of the tricritical point are in agreement with results of refs. 18 and 19. The discrepancy of this result with the results of Monte Carlo simulations and perturbations methods where a nonuniversal critical behavior is found —for a list of references see ref. 19, may be an artifact of the CVM approximation.

3.2. The Correlation Function

For the calculation of the correlation function it is convenient to write the free energy (10) as a function of the parameters

$$\begin{aligned} m_x &= \mathrm{Tr}(\sigma_x \rho_x) \\ l_{xy} &= \mathrm{Tr}(\sigma_x \sigma_y \rho_{\langle xy \rangle}) \\ c_{xy} &= \mathrm{Tr}(\sigma_x \sigma_y \rho_{\ll xy \gg}) \\ k_{xyz} &= \mathrm{Tr}(\sigma_x \sigma_y \sigma_z \rho_{[xyz]}) \\ d_{xywz} &= \mathrm{Tr}(\sigma_x \sigma_y \sigma_w \sigma_z \rho_{y \square z}^{x \; w}) \end{aligned} \tag{11}$$

that are related to the density matrices by:

$$\begin{aligned} \rho_x &= \tfrac{1}{2}(1 + m_x \sigma_x) \\ \rho_{\langle xy \rangle} &= \tfrac{1}{4}(1 + m_x \sigma_x + m_y \sigma_y + l_{xy} \sigma_x \sigma_y) \\ \rho_{\ll xy \gg} &= \tfrac{1}{4}(1 + m_x \sigma_x + m_y \sigma_y + c_{xy} \sigma_x \sigma_y) \\ \rho_{y \square z}^{x \; w} &= \tfrac{1}{16}(1 + m_x \sigma_x + m_y \sigma_y + m_w \sigma_w + m_z \sigma_z \\ &\quad + l_{xw} \sigma_x \sigma_w + l_{wz} \sigma_w \sigma_z + l_{zy} \sigma_z \sigma_y + l_{yx} \sigma_y \sigma_x \\ &\quad + c_{xz} \sigma_x \sigma_z + c_{yw} \sigma_y \sigma_w + k_{yxw} \sigma_y \sigma_x \sigma_w \\ &\quad + k_{xwz} \sigma_x \sigma_w \sigma_z + k_{wzy} \sigma_w \sigma_z \sigma_y \\ &\quad + k_{zyx} \sigma_z \sigma_y \sigma_x + d_{xywz} \sigma_x \sigma_w \sigma_z \sigma_y) \end{aligned} \tag{12}$$

We have seen in Section II that in order to calculate the pair correlation function, we need to evaluate the matrix

$$\left(\frac{\partial h_x}{\partial m_y}\right)_{m_z=0\ \forall z} \tag{13}$$

Therefore we consider the state equation for the magnetization $\partial \mathscr{F}/\partial m_i = 0$:

$$\beta h_i = -\tfrac{1}{4}\sum_{\langle iy\rangle} \mathrm{Tr}(\sigma_i \log \rho_{\langle iy\rangle}) + \tfrac{1}{16}\sum_{\substack{i\\ y\square z}}^{w} \mathrm{Tr}(\sigma_i \log \rho_{\substack{i\\ y\square z}}^{w}) + \tfrac{1}{2}\mathrm{Tr}(\sigma_i \log \rho_i) \tag{14}$$

where the first and the second sums are respectively taken over the pairs of nearest neighbors and the plaquettes containing the site i. We start from the diagonal elements of the matrix (13) given by

$$\begin{aligned}\beta \frac{\partial h_i}{\partial m_i} = &-\frac{1}{16}\sum_{\langle iy\rangle} \mathrm{Tr}\left(\frac{1}{\rho_{\langle iy\rangle}}\right) + \frac{1}{4}\mathrm{Tr}\left(\frac{1}{\rho_i}\right)\\ &+\frac{1}{256}\sum_{\substack{i\\ y\square z}}^{w} \mathrm{Tr}\left[\frac{\sigma_i}{\rho_{\substack{i\\ y\square z}}^{w}}\left(\sigma_i + \sigma_y\sigma_z\sigma_w \frac{\partial k_{yzw}}{\partial m_i}\right.\right.\\ &\left.\left.+ 2\sigma_i\sigma_y\sigma_z \frac{\partial k_{iyz}}{\partial m_i} + \sigma_w\sigma_i\sigma_y \frac{\partial k_{wiy}}{\partial m_i}\right)\right]\end{aligned} \tag{15}$$

where all the derivatives are evaluated in $m_z = 0\ \forall z$ and $\partial k_{zwi}/\partial m_i = \partial k_{iwz}/\partial m_i$ has been assumed. Derivatives like $\partial l_{xy}/\partial m_i$, $\partial c_{xy}/\partial m_i$, $\partial d_{xywz}/\partial m_i$ do not appear because they are odd functions of m_i evaluated at $m_i = 0$. Moreover in the paramagnetic phase $l_{xy} = l$, $c_{xy} = c$ and $d_{xywz} = d\ \forall x, y, w, z$. To simplify the notation we introduce

$$k_1 = \frac{\partial k_{iyz}}{\partial m_i}, \qquad k_2 = \frac{\partial k_{wiy}}{\partial m_i} \qquad \text{and} \qquad k_3 = \frac{\partial k_{yzw}}{\partial m_i} \tag{16}$$

While the parameters l, c and d can be calculated as usual by solving the equilibrium state equations by means of the Natural Iteration Method, the calculation of k_1, k_2 and k_3 is a little bit more intriguing. As explained in Section II it is convenient to consider the state equation obtained by setting equal to zero the derivative of the free energy with respect to k_{xyz}

$$\mathrm{Tr}(\sigma_x\sigma_y\sigma_z \log \rho_{\substack{x\\ y\square z}}^{w}) = 0 \tag{17}$$

Now, by differentiating this equation with respect to m_j with $j = x, y, w$, we obtain the system:

$$\mathrm{Tr}\left[\frac{\sigma_x\sigma_y\sigma_z}{\rho_{y\square z}^{x\square w}}\left(\sigma_j + \sum_{[x',y',z']\subset {}_{y}^{x}\square_{z}^{w}} \sigma_{x'}\sigma_{y'}\sigma_{z'}\frac{\partial k_{x'y'z'}}{\partial m_j}\right)\right] = 0 \quad j = x, y, w \tag{18}$$

By solving this system of three equations in the variables k_1, k_2 and k_3 one obtains

$$\begin{aligned} k_1 &= \frac{A(C-D)}{(D+B+2A)(D+B-2A)} \\ k_2 &= \frac{(C-D)(B^2+BD-2A^2)}{(D-B)(D+B+2A)(D+B-2A)} \\ k_3 &= \frac{2A^2(C+D-2B)+(B^2-DC)(B+D)}{(D-B)(D+B+2A)(D+B-2A)} \end{aligned} \tag{19}$$

where

$$\begin{aligned} A &= \mathrm{Tr}\left(\frac{\sigma_x\sigma_y}{\rho_{y\square z}^{x\square w}}\right); \qquad B = \mathrm{Tr}\left(\frac{\sigma_y\sigma_w}{\rho_{y\square z}^{x\square w}}\right) \\ C &= \mathrm{Tr}\left(\frac{\sigma_x\sigma_y\sigma_w\sigma_z}{\rho_{y\square z}^{x\square w}}\right); \qquad D = \mathrm{Tr}\left(\frac{1}{\rho_{y\square z}^{x\square w}}\right) \end{aligned} \tag{20}$$

The insertion of Eqs. (19), (20) in (15) gives the diagonal elements of (13). Going further, by differentiating (14) with respect to m_j with i, j nearest neighbours, one realizes that derivatives like $\partial k_{ixy}/\partial m_j$ with $j \notin {}_{y}^{x}\square_{z}^{i}$ appear. However, these derivatives are zero. Indeed, by differentiating the state equation for k_{xyz} with respect to m_j with j external to the plaquette of $[xyz]$, we obtain an equation similar to (18) but without the first term σ_j in circular brackets. Changing the site j we again obtain a systems for the derivatives $\partial k_{xyz}/\partial m_j$ with j external to the plaquette of $[xyz]$, but in this case these derivatives are zero since the system is homogeneous.

A consequence of the above considerations is that the matrix (13) can be written as

$$\beta\left(\frac{\partial h_i}{\partial m_y}\right)_{m_z=0\ \forall z} = \begin{cases} \gamma & i = y \\ -\gamma_1 & \langle iy\rangle \\ -\gamma_2 & \langle\langle iy\rangle\rangle \\ 0 & \text{otherwise} \end{cases} \tag{21}$$

with

$$\gamma = 1 - \frac{4}{1-l^2} + (1+k_2+k_3)\frac{1+2c+d}{(1+4l+2c+d)(1-4l+2c+d)} + (1-k_2+k_3)\frac{1}{1-2c+d} + (1-k_3)\frac{2}{1-d} - \frac{8k_1 l}{(1+4l+2c+d)(1-4l+2c+d)} \tag{22}$$

$$-\gamma_1 = \frac{l}{1-l^2} - \frac{2l}{(1+4l+2c+d)(1-4l+2c+d)} + k_1\left(\frac{1+2c+d}{(1+4l+2c+d)(1-4l+2c+d)} - \frac{1}{1-d}\right) - \frac{2(k_2+k_3)\,l}{(1+4l+2c+d)(1-4l+2c+d)} \tag{23}$$

and

$$-\gamma_2 = \frac{1}{4}(1+k_2+k_3)\frac{1+2c+d}{(1+4l+2c+d)(1-4l+2c+d)} - \frac{1}{4}(1-k_2+k_3)\frac{1}{1+2c+d} - \frac{k_2}{2(1-d)} - \frac{2k_1 l}{(1+4l+2c+d)(1-4l+2c+d)} \tag{24}$$

The inverse of the Fourier transform of the matrix (21) gives the pair correlation function in Fourier space, or structure factor. It reads as

$$S(\mathbf{p}) = \frac{1}{\gamma - 2\gamma_1 \sum_{\mu=1}^{2} \cos(p_\mu) - 2\gamma_2(\cos(p_1+p_2)+\cos(p_1-p_2))} \tag{25}$$

3.3. The Disorder Line

The line where the coefficient of p^2 in the denominator of (25) is zero is the so called Lifshitz line where the structure factor develops a maximum at a value of p different from zero. It is given by $\gamma_1 + 2\gamma_2 = 0$ and is reported in Fig. 1. The other interesting line for the behavior of the correlation function is the disorder line where the correlation in real space changes its behavior from a purely exponential decay to an oscillating exponentially

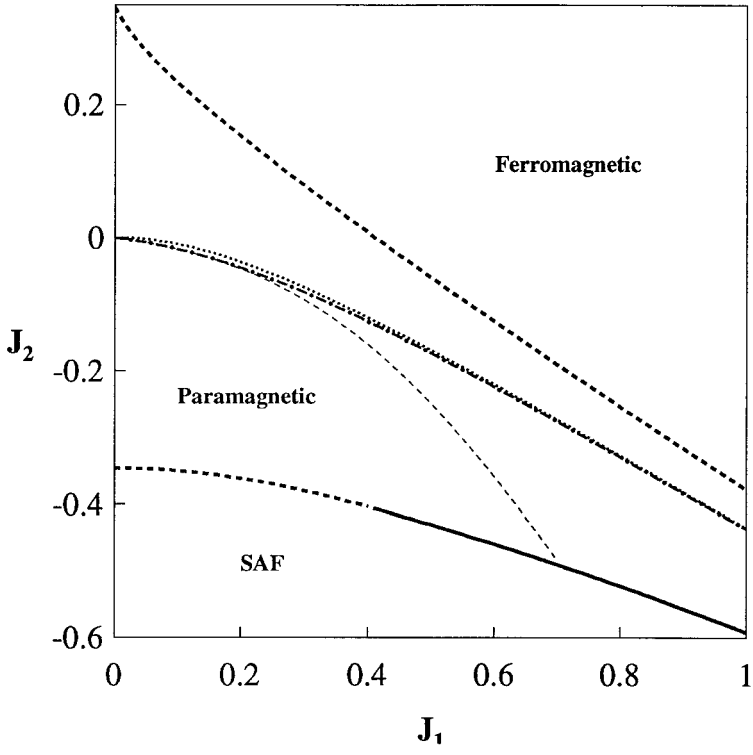

Fig. 1. Phase diagram of model (9) in $D=2$ with $J_3=0$. The dashed lines are critical lines separating the disordered phase from the ferromagnetic and the lamellar (SAF) phases. The first-order transition between the paramagnetic and SAF phases is represented by a solid line. The dotted line is the one-dimensional line of equation (28), while the light dashed and dash-dotted lines are the mean field and plaquette approximation calculation of the disorder line, respectively.

decay. In order to calculate this line it is convenient to take the spherical average of the expansion of (25) at small $\vec{p}$ so that the structure factor can be written as:[20]

$$S(\mathbf{p}) = \frac{S(0)}{1 + bp^2 + cp^4} \tag{26}$$

The spherical average can be simply realized by expanding (25) until the fourth power of $\vec{p}$ and taking $p_x = p_y = p/\sqrt{2}$.[20] The result is

$$b = \frac{\gamma_1 + 2\gamma_2}{\gamma - 4(\gamma_1 + \gamma_2)}; \qquad c = -\frac{1}{24}\frac{\gamma_1 + 8\gamma_2}{\gamma - 4(\gamma_1 + \gamma_2)} \tag{27}$$

On the disorder line the zero of the denominator of (25) changes from pure imaginary to complex. This happens when $b^2 - 4c = 0$. In Fig. 1 we plot the disorder line obtained by Eqs. (27).

In some bidimensional model with competing interactions the disorder line coincides with a locus (One-Dimensional-Line) where the model can be solved exactly and has typical one-dimensional correlations.[21] The ODL line has been calculated for the model (9) with $J_3 = 0$ and is given by[22]

$$\cosh 2J_1 = \frac{e^{4J_2} + e^{-4J_2} + 2e^{-2J_2}}{2(1 + e^{2J_2})} \tag{28}$$

It would be interesting to know whether this line, also reported in Fig. 1, coincides with the disorder line of the model (9). In ref. 23 the ODL line has been compared to the disorder line obtained in mean field approximation. Here we have an approximation which correctly reproduce the topology of the phase diagram of the model also at low temperatures. This allows us to compare our approximation for the disorder line with the expression (28) at any value of J_1, J_2. We see that the disorder line calculated by CVM is very close to the ODL Eq. (28), so that it is probably true that the two lines coincide. For further comparison we have plotted in Fig. 1 also the disorder line obtained by mean-field approximation.

IV. THE 3D ISING MODEL WITH NN, NNN AND PLAQUETTE INTERACTIONS

In this section we study in the CVM approximation the phase diagram and the disorder line of the model (9) defined on the cubic lattice. The ground states of the model (9) are shown in Fig. 2. They can be simply obtained by minimizing for each value of the parameters J_1, J_2, J_3 the energy of a single cube.[10] When two or more cube configurations have the same minimum energy, it may be possible to construct a set of degenerate ground states by tiling the whole lattice with the degenerate cube configurations. We have chosen to study the particular cases $J_2 = J_3$ and $J_3 = -2J_2$ since in these cases the structure of the ground states is of particular interest for the applications.[10, 11] The diagrams of the ground states for these cases are shown in Fig. 3.

Due to the fact that the ground states can be expressed in terms of single cube configurations, it is necessary for a correct implementation of the CVM approximation to consider the cube with 8 independent site

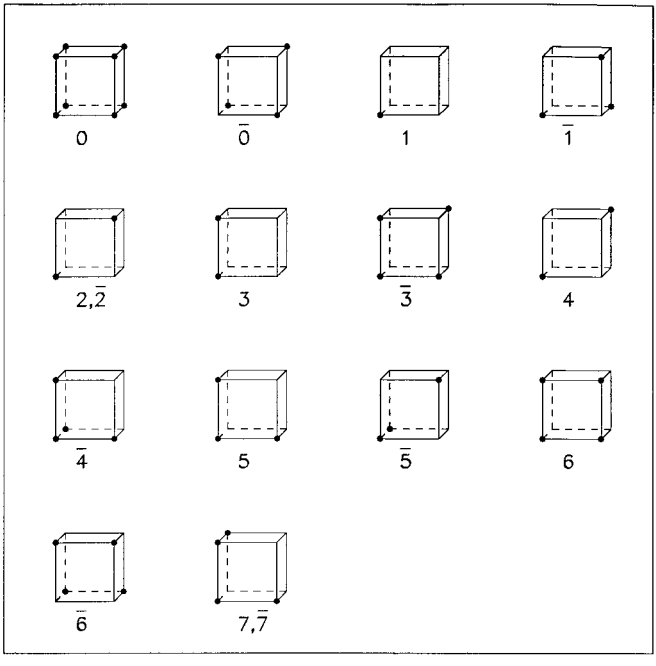

Fig. 2. Ground states of the 3D model. The dot • indicates $\sigma = +1$ while $\sigma = -1$ in the remaining sites. The labels refer both to the phase and to the dotted subclusters. The complementary (non-dotted) subclusters can be referred to adding a "c" after the label.

magnetizations as the maximal cluster in the CVM implementation. Then the approximated free-energy is given by

$$\begin{aligned}\beta\mathscr{F} = &-J_1 \sum_{\langle xy\rangle} \mathrm{Tr}(\sigma_x\sigma_y\rho_{\langle xy\rangle}) - J_2 \sum_{\langle\langle xy\rangle\rangle} \mathrm{Tr}(\sigma_x\sigma_y\rho_{\langle\langle xy\rangle\rangle}) \\ &- J_3 \sum_{\substack{x \\ y\square z}}^{w} \mathrm{Tr}(\sigma_x\sigma_y\sigma_w\sigma_z\rho_{\substack{x \\ y\square z}}^{w}) - \beta \sum_x h_x \,\mathrm{Tr}(\sigma_x\rho_x) + \sum_c \mathrm{Tr}\,\mathscr{L}(\rho_c) \\ &- \sum_{\substack{x \\ y\square z}}^{w} \mathrm{Tr}\,\mathscr{L}(\rho_{\substack{x \\ y\square z}}^{w}) + \sum_{\langle xy\rangle} \mathrm{Tr}\,\mathscr{L}(\rho_{\langle xy\rangle}) - \sum_x \mathrm{Tr}\,\mathscr{L}(\rho_x) \end{aligned} \tag{29}$$

where ρ_c is the density matrix of an elementary cube. Also here, as in the bidimensional case, the coefficients of the entropic terms have been found by applying the prescriptions of ref. 2.

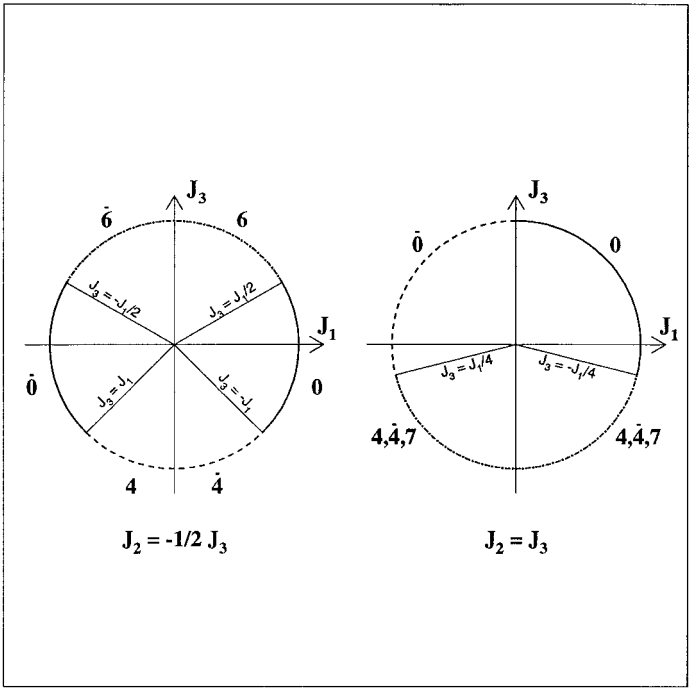

Fig. 3. Ground states of the 3D model for the values $J_2 = J_3$ and $J_2 = -J_3/2$ of the coupling constants.

4.1. The Phase Diagram with $J_2 = J_3$

This case has been studied in refs. 10, 11 by using mean-field approximation and Monte Carlo simulations. In terms of dual surfaces, it corresponds to the case where the curvature, defined as the number of adjacent plaquettes forming a right angle, is not weighted.[10] The phase diagram found by applying the natural iteration scheme to the CVM free-energy (29) is shown in Fig. 4. At positive J_2 the ferromagnetic phase is stable. On the transition line separating the ferromagnetic and the paramagnetic phases there is a tricritical point at $J_1^{tr} = 0.029$, $J_2^{tr} = 0.0635$. The coordinates of the tricritical point in mean field approximation and by Monte Carlo simulations are respectively given by $J_1^{tr,\,MF} = 0.11$, $J_2^{tr,\,MF} = 0.0275$, $J_1^{tr,\,MC} = 0.03$, $J_2^{tr,\,MC} = 0.064$. A relevant difference between the mean-field and the CVM phase diagram is that in the CVM approximation the paramagnetic phase extends until zero temperature, in agreement with results of Monte Carlo simulations. At negative J_2 the ordered stable configurations can be constructed starting by the cubes in Fig. 5. The phase between the phases $\bar{4}$

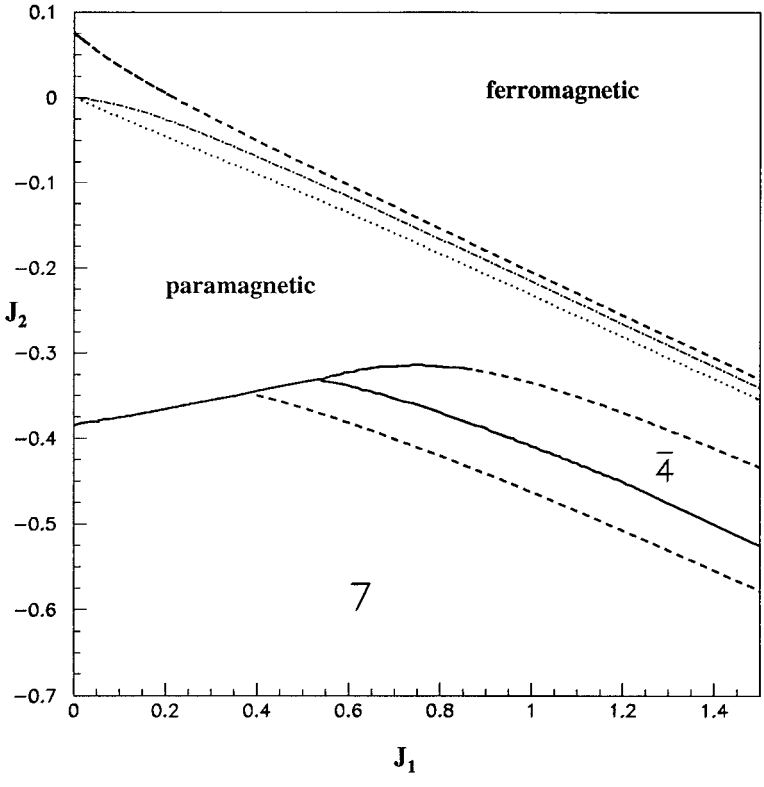

Fig. 4. Phase diagram of model (9) in $D=3$ with $J_3=J_2$. The dash-dotted line is the disorder line in cube approximation. The dotted line is the Lifshitz line. In the narrow strip between the 7 and $\bar{4}$ phases we find a type-7 phase with the magnetizations m of Fig. 5 equal to zero. As before, solid and dashed lines represent first-order and critical transition lines.

and 7 in Fig. 4 has the same configuration of phase 7 but with the magnetizations $m=0$. This phase is separated from the phases $\bar{4}$ and 7 by a first-order and a critical line, respectively. The phases $\bar{4}$ and 7 are bicontinuous in the sense that the domains of spins of one sign form a connected network invading all the lattice and intertwined with the network formed by the spins of the other sign.[10] Also mean field and Monte Carlo simulations show stable bicontinuous configuration in this region. However, there are discrepancies between the phase diagrams obtained by different methods at $J_2<0$. The origin of the discrepancies is probably in the particular nature of the ground states at $J_2<-|J_1|/4$. As it can be seen from Fig. 3, the cube configurations 4, $\bar{4}$, 7 are degenerate for $J_2<-|J_1|/4$ and an infinite number of bicontinuous ground states can be built up using these configurations. Here, probably, a low-temperature expansion is

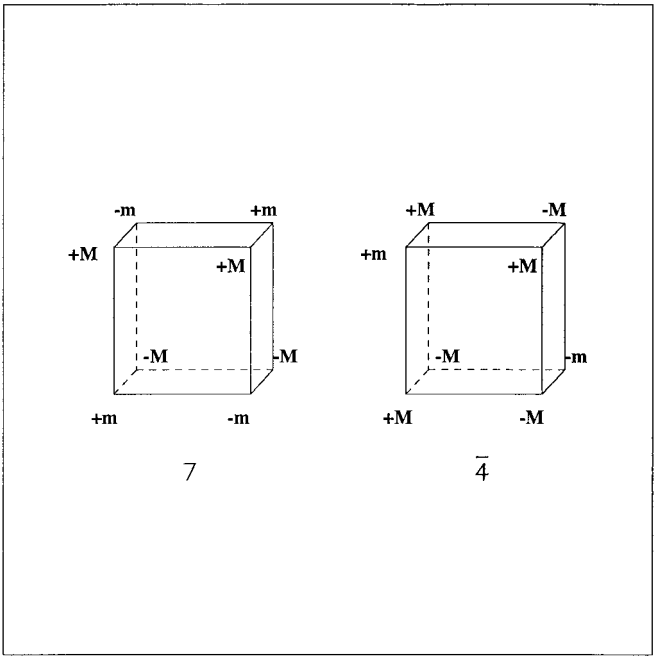

Fig. 5. Phases at finite temperature appearing in the diagram of Fig. 4. Capital letters indicate bigger magnetizations.

needed to understand the correct nature of the stable phases, but this will be the matter for a future study. It is interesting to observe that on the transition line between the paramagnetic phase and the $\bar{4}$ phase at negative J_2 there is a tricritical point located at $J_1 = 0.87, J_2 = -0.32$. It would be interesting to check the existence of this tricritical point by Monte Carlo simulations.

4.2. The Disorder Line

In three-dimensions the calculation of the disorder line proceeds in the same two steps as in the bidimensional case but with complications due to the higher number of variational parameters in the ρ_c expansion. This implies the existence of many terms like the quantities k_1, k_2, etc. of the previous section to evaluate.

The first step is the calculation of the elements of the inverse correlation matrix (13), that in tree dimensions becomes

$$\beta\left(\frac{\partial h_i}{\partial m_y}\right)_{m_z=0\ \forall z} = \begin{cases} \gamma & i=y \\ -\gamma_1 & \langle iy\rangle \\ -\gamma_2 & \langle\langle iy\rangle\rangle \\ -\gamma_3 & \langle\langle\langle iy\rangle\rangle\rangle \\ 0 & \text{otherwise} \end{cases} \tag{30}$$

The explicit expressions of the coefficients γ_i are given in Appendix A for clearness purposes. Going on with the second part of the calculation, we use these matrix elements to compute the coefficients (27) of the small-$\vec{p}$ expansion of the structure factor, that in three dimensions are given by:

$$b = \frac{\gamma_1 + 4\gamma_2 + 4\gamma_3}{\gamma - 6\gamma_1 - 12\gamma_2 - 8\gamma_3}; \qquad c = -\frac{1}{36}\frac{\gamma_1 + 16\gamma_2 + 28\gamma_3}{\gamma - 6\gamma_1 - 12\gamma_2 - 8\gamma_3} \tag{31}$$

Also here, as in the bidimensional case, a spherical average has been performed taking $p_x = p_y = p_z = p/\sqrt{3}$. When $b^2 - 4c < 0$ the correlation function in real space is given by

$$G(r) = \frac{\text{const}}{r} e^{-r/\xi} \sin\frac{2\pi r}{\delta} \tag{32}$$

where

$$\delta = \frac{2\pi}{[(1/2\sqrt{c}) + (b/4c)]^{1/2}} \qquad \xi = \frac{1}{[(1/2\sqrt{c}) - (b/4c)]^{1/2}} \tag{33}$$

The disorder line corresponds to the condition $b^2 - 4c = 0$. The results for the disorder line and for the Lifshitz line $b = 0$ are shown in Fig. 4. At low temperatures both the lines behave as $J_2 = -J_1/4$.

4.3. The Phase Diagram at $J_3 = -2J_2$

The ground-state structure corresponding to this case is shown in Fig. 3. We see that the ferromagnetic phase is bounded from a phase with spin of different sign in alternate planes. We call this last phase a lamellar phase. At finite temperature the phase diagram has been studied in mean field approximation in a previous paper.[11] It can well describe the phase diagram of experimental mixtures of oil, water, and surfactant. The CVM approximation is the same used before and the calculation of the disorder line also proceeds in the way already discussed in the preceding paragraph

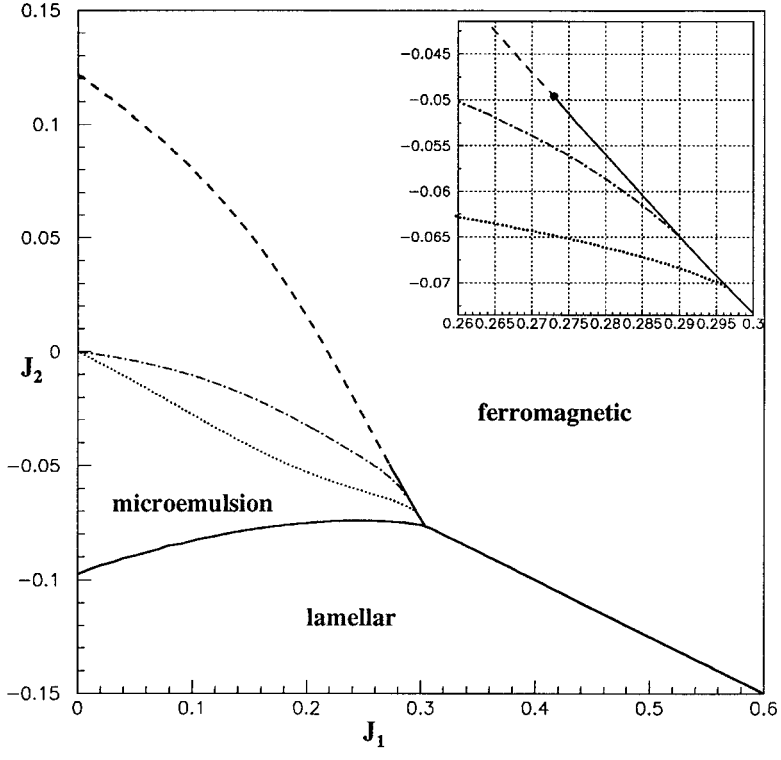

Fig. 6. Phase diagram of model (9) in $D=3$ with $J_3=-2J_2$. The dash-dotted line is the disorder line; the dotted line is the Lifshitz line. In the inset, the region where the disorder and the Lifshitz lines cross the first-order Ferro-Paramagnetic transition line is enlarged.

of this section. Therefore we can go on by describing the phase diagram shown in Fig. 6.

At low temperatures and positive J_2 the stable phase is the ferromagnetic one, while for negative J_2 we find the lamellar phase being stable. On the transition line between the ferromagnetic and the paramagnetic phases there is a tricritical point at $J_1=0.273$, $J_2=-0.049$, with the first-order part of the line joining the boundary of the lamellar phase region at $J_1=0.305$, $J_2=-0.077$ (4-phase point). This feature, together with the observation that the disorder line intersects the first-order ferro-paramagnetic transition line in $J_1=0.29$, $J_2=-0.065$, between the tricritical and the 4-phase point, well represents the experimental fact that the microemulsion phase (corresponding to the region of the paramagnetic phase below the disorder line) can coexist with the ordered homogeneous phases.[11, 16] We also observe that the Lifshitz line intersects the ordered

phases at the point $J_1 = 0.2965 \pm 0.0005$; $J_2 = -0.00705 \pm 0.00005$. The region close to the 4-phase point is shown in the inset of Fig. 6.

V. CONCLUSIONS

The CVM approximation is generally used for studying the topology of phase diagrams of spin systems. In this paper we have focused on the calculation of the correlation functions in the framework of this approximation. This calculation can become complicate expecially in the case of three-dimensional systems and we have discussed the origin of these complications. As particular models we have considered the Ising model with NN, NNN, and plaquette interactions on the square and on the cubic lattice. We have calculated the pair correlation function in the paramagnetic phase of these models. We have also given new results about the phase diagrams of these models for choices of parameters useful for the description of experimental systems.

In particular, in the two-dimensional case with zero plaquette interaction, we have calculated the disorder line in the paramagnetic phase and we have seen that it is very close to the One-Dimensional Line where the model is exactly solvable. This strengthens the conjecture that the disorder line and the ODL, line coincide also in this model. In the three-dimensional case we have chosen two planes in the parameter space where the phase diagram may have a relevance for the description of systems of interacting surfaces with fluctuating topology. Fluid mixtures of oil, water, and surfactant are an example of these systems. We have calculated the disorder line and the Lifshitz line which limit regions of the paramagnetic phase detectable through scattering experiments. Our results, shown in Figs. 4 and 6 confirm that the three-dimensional Ising model with NN, NNN, and plaquette interactions can describe many of the experimental features appearing in complex fluid mixtures.

VI. APPENDIX A

The matrix (30) can be evaluated through the same procedure shown in Section III, starting from the single spin magnetization state equation (14), that in 3D turns out to be:

$$\beta h_i = \tfrac{1}{256} \sum_{c \ni i} \mathrm{Tr}(\sigma_i \log \rho_c) - \tfrac{1}{16} \sum_{\substack{i \\ y \square z}}^{w} \mathrm{Tr}(\sigma_i \log \rho_{\substack{i \\ y \square z}}^{w}) + \tfrac{1}{4} \sum_{\langle iy \rangle} \mathrm{Tr}(\sigma_i \log \rho_{\langle iy \rangle}) - \tfrac{1}{2} \mathrm{Tr}(\sigma_i \log \rho_i) \tag{34}$$

Differentiating this equation with respect to the site magnetizations, we realize that we have to deal with a long list of derivatives of the kind: $D_i^{\alpha} = \partial \xi_{\alpha} / \partial m_i$ where $\xi_{\alpha} = \mathrm{Tr}(\sigma_{\alpha} \rho_{\alpha})$ is the parameter in the expansion of the density matrix corresponding to the subcluster α. By symmetry considerations and taking into account that in the paramagnetic phase the only derivatives different from zero are those from subclusters with an odd number of sites, we can reduce the number of derivatives to 33, listed in Fig. 7. Repeating the procedure used in Section III to obtain (18), we can get to a system of 33 linear equations which, although very long, can be straightforwardly solved and it will not be reported here. The solution of this system gives us the coefficients k_i, a_i, b_i appearing in Fig. 7 and allows

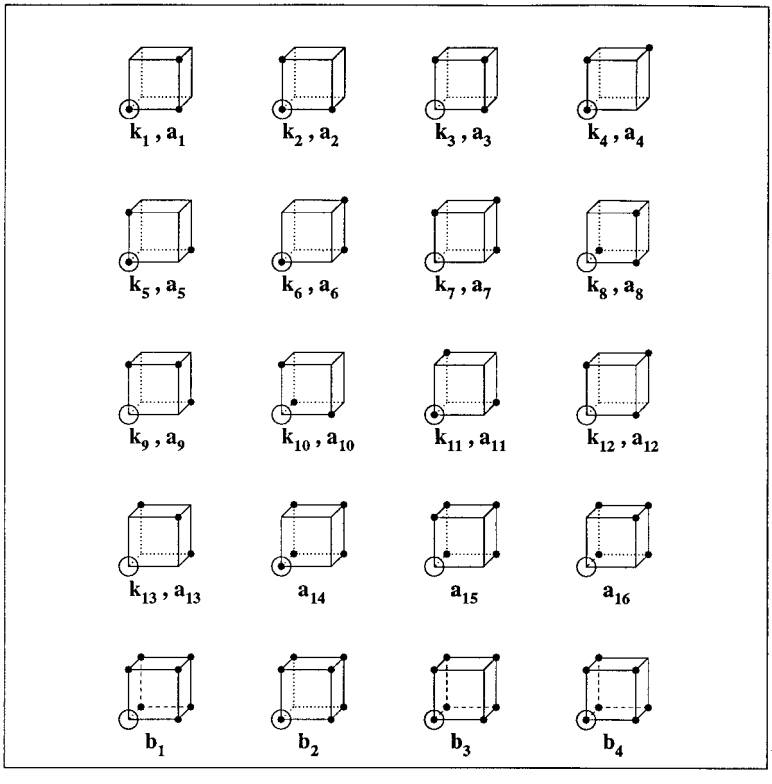

Fig. 7. Derivatives $D_i^{\alpha} = \partial \xi_{\alpha} / \partial m_i$ with respect to the magnetization m_i in the site circled (see App. A for the notations). k_i, a_i, and b_i are respectively the derivatives of the 3-, 5- and 7-sites subclusters, represented by the dots. From $k_1(a_1)$ to $k_3(a_3)$ the cluster considered is $\alpha = 5(5c)$; from $k_4(a_4)$ to $k_9(a_9)$, $\alpha = \bar{5}(\bar{5}c)$, from $k_{10}(a_{10})$ to $k_{13}(a_{13})$, $\alpha = \bar{1}(\bar{1}c)$, from a_{14} to a_{16}, $\alpha = 5c$ and there is no correpsonding k_i; from b_1 to b_4, $\alpha = 1c$.

us to calculate the expression of the matrix elements (30), that we write down here explicitly:

$$\begin{aligned}
\gamma = 8[\, & C^{0c} + 6k_1 C^3 + 3k_2 C^2 + 3k_3 C^6 + 3k_4 C^2 \\
& + 3k_5 C^4 + 3k_6 C^3 + 3k_7 C^{\bar{6}} \\
& + 6k_8 C^7 + 6k_9 C^{\bar{3}} + k_{10} C^{\bar{4}} + 3k_{11} C^2 + 3k_{12} C^{\bar{3}} \\
& + k_{13} C^{\bar{0}} + 6a_1 C^{3c} + 3a_2 C^{2c} \\
& + 3a_3 C^6 + 6a_{14} C^7 + 3a_{15} C^{\bar{4}} + 3a_{16} C^{\bar{3}} \\
& + 3a_4 C^{2c} + 3a_5 C^{4c} + 3a_6 C^{3c} + 3a_7 C^{\bar{6}} \\
& + 6a_8 C^7 + 6a_9 C^{\bar{3}} + a_{10} C^{3c} + 3a_{11} C^{2c} \\
& + 3a_{12} C^{\bar{3}} + a_{13} C^{\bar{0}} + b_1 C^0 + 3b_2 C^{3c} + 3b_3 C^{2c} + b_4 C^{4c}] \\
& - 12[\, P^{0c} + 2k_1 P^1 + k_2 P^2 + k_3 P^0] + 6L^{0c} - 1
\end{aligned} \tag{35}$$

$$\begin{aligned}
-\gamma_1 = 4[\, & C^3 + 2k_1(C^2 + C^6 + C^7) + k_2(2C^3 + C^{\bar{4}}) \\
& + k_3(2C^3 + C^{\bar{3}}) + k_4(C^4 + 2C^{\bar{3}}) \\
& + k_5(C^2 + 2C^7) + k_6(2C^7 + C^{\bar{6}}) + k_7(C^3 + 2C^{\bar{3}}) \\
& + 2k_8(C^3 + C^4 + C^{\bar{3}}) + 2k_9(C^2 + C^7 + C^{\bar{6}}) \\
& + k_{10} C^2 + k_{11}(C^{\bar{4}} + C^{\bar{3}}) + k_{12}(2C^2 + C^{\bar{0}}) \\
& + k_{13} C^{\bar{3}} + 2a_1(C^{2c} + C^6 + C^7) \\
& + a_2(2C^{3c} + C^{\bar{4}}) + a_3(2C^{3c} + C^{\bar{3}}) \\
& + 2a_{14}(C^{3c} + C^{\bar{4}} + C^{\bar{3}}) + a_{15}(C^{2c} + 2C^7) \\
& + a_{16}(C^6 + 2C^7) + a_4(C^4 + 2C^{\bar{3}}) + a_5(C^2 + 2C^7) \\
& + a_6(2C^7 + C^{\bar{6}}) + a_7(C^3 + 2C^{\bar{3}}) \\
& + 2a_8(C^3 + C^4 + C^{\bar{3}}) + 2a_9(C^2 + C^7 + C^{\bar{6}}) + a_{10} C^2 + a_{11}(C^{\bar{4}} + C^{\bar{3}}) \\
& + a_{12}(2C^2 + C^{\bar{0}}) + a_{13} C^{\bar{3}} + b_1 C^{3c} + b_2(C^0 + 2C^{2c}) \\
& + b_3(2C^{3c} + C^{4c}) + b_4 C^{2c}] \\
& - 4[\, P^1 + k_1(P^2 + P^0) + k_2 P^1 + k_3 P^1] + L^0
\end{aligned} \tag{36}$$

$$
\begin{aligned}
-\gamma_2 = 2[\, & C^2 + 2k_1(C^3 + C^{\bar 4} + C^{\bar 3}) + k_2(C^6 + 2C^7) \\
& + k_3(C^2 + 2C^7) + k_4(2C^7 + C^{\bar 6}) \\
& + k_5(C^3 + 2C^{\bar 3}) + k_6(C^4 + 2C^{\bar 3}) \\
& + k_7(C^2 + 2C^7) + 2k_8(C^2 + C^7 + C^{\bar 6}) \\
& + 2k_9(C^3 + C^4 + C^{\bar 3}) + k_{10} C^{\bar 3} \\
& + k_{11}(2C^2 + C^{\bar 0}) + k_{12}(C^{\bar 4} + 2C^{\bar 3}) + k_{13} C^2 \\
& + 2a_1(C^{3c} + C^{\bar 4} + C^{\bar 3}) + a_2(C^6 + 2C^7) + a_3(C^{2c} + 2C^7) \\
& + 2a_{14}(C^{2c} + C^6 + C^7) \\
& + a_{15}(2C^{3c} + C^{\bar 3}) + a_{16}(2C^{3c} + C^{\bar 4}) + a_4(2C^7 + C^{\bar 6}) + a_5(C^{3c} + 2C^{\bar 3}) \\
& + a_6(C^{4c} + 2C^{\bar 3}) + a_7(C^{2c} + 2C^7) + 2a_8(C^{2c} + C^7 + C^{\bar 6}) \\
& + 2a_9(C^{3c} + C^{4c} + C^{\bar 3}) \\
& + a_{10} C^{\bar 3} + a_{11}(2C^{2c} + C^{\bar 0}) + a_{12}(C^{\bar 4} + 2C^{\bar 3}) \\
& + a_{13} C^{2c} + b_1 C^{2c} + b_2(C^{4c} + 2C^{3c}) \\
& + b_3(C^0 + 2C^{3c}) + b_4 C^{3c}] - [P^2 + 2k_1 P^1 + k_2 P^0 + k_3 P^2]
\end{aligned} \tag{37}
$$

$$
\begin{aligned}
-\gamma_3 = {} & C^4 + 6k_1 C^7 + 3k_2 C^{\bar 3} + 3k_3 C^{\bar 4} + 3k_4 C^{0c} \\
& + 3k_5 C^{\bar 6} + 3k_6 C^2 + 3k_7 C^4 + 6k_8 C^{\bar 3} \\
& + 6k_9 C^{\bar 3} + k_{10} C^{\bar 0} + 3k_{11} C^{\bar 3} + 3k_{12} C^2 + k_{13} C^{\bar 4} \\
& + 6a_1 C^7 + 3a_2 C^{\bar 3} + 3a_3 C^{\bar 4} \\
& + 6a_{14} C^{3c} + 3a_{15} C^6 + 3a_{16} C^{2c} + 3a_4 C^{0c} + 3a_5 C^{\bar 6} \\
& + 3a_6 C^{2c} + 3a_7 C^{4c} + 6a_8 C^{\bar 3} \\
& + 6a_9 C^{\bar 3} + a_{10} C^{\bar 0} + 3a_{11} C^{\bar 3} + 3a_{12} C^{2c} + a_{13} C^{\bar 4} \\
& + b_1 C^{4c} + 3b_2 C^{2c} + 3b_3 C^{3c} + b_4 C^0
\end{aligned} \tag{38}
$$

where we used the notations: $P^0 = \frac{1}{256}\,\mathrm{Tr}(\sigma_x\sigma_y\sigma_z\sigma_w/\rho_{\frac{x}{y}\square\frac{w}{z}})$, $P^1 = \frac{1}{256}\,\mathrm{Tr}(\sigma_i\sigma_j/\rho_{\frac{i}{j}\square\frac{w}{z}})$, $P^2 = \frac{1}{256}\,\mathrm{Tr}(\sigma_i\sigma_j/\rho_{\frac{i}{y}\square\frac{w}{j}})$, $P^{0c} = \frac{1}{256}\,\mathrm{Tr}(1/\rho_{\frac{x}{y}\square\frac{w}{z}})$, $L^0 = \frac{1}{16}\,\mathrm{Tr}(\sigma_x\sigma_y/\rho_{\langle xy\rangle})$, $L^{0c} = \frac{1}{16}\,\mathrm{Tr}(1/\rho_{\langle xy\rangle})$ and $C^\alpha = (1/(256)^2)\,\mathrm{Tr}(\sigma_\alpha/\rho_c)$, α being the name of the cluster as they are classified in Fig. 2, and $\sigma_\alpha = \prod_{i\in\alpha}\sigma_i$, as in Section II.

REFERENCES

1. R. Kikuchi, *Phys. Rev.* **81**:988 (1951).
2. G. An, *J. Stat. Phys.* **52**:727 (1988); T. Morita, *J. Stat. Phys.* **59**:819 (1990).
3. We observe that the CVM has also been used in combination with Padé approximants to estimate critical exponents. See A. Pelizzola, *Phys. Rev. E* **49**:R2503 (1994); *ib.* **53**:5825 (1996).
4. See, e.g., A. Pelizzola, *Physica A* **211**:107 (1994).
5. J. M. Sanchez, *Physica* **111A**:200 (1982).
6. A. Finel and D. de Fontaine, *J. Stat. Phys.* **43**:645 (1986).
7. R. Kikuchi, *J. Chem. Phys.* **60**:1071 (1974).
8. R. J. Baxter, *Exactly Solved Models in Statistical Mechanics* (Academic Press, London, 1982).
9. M. Karowski, *J. Phys. A* **19**:3375 (1986).
10. A. Cappi, P. Colangelo, G. Gonnella, and A. Maritan, *Nucl. Phys. B* **370**:659 (1992).
11. G. Gonnella, S. Lise, and A. Maritan, *Europhys. Lett.* **32**:735 (1995).
12. P. Colangelo, G. Gonnella, and A. Maritan, *Phys. Rev. E* **47**:411 (1993).
13. R. V. Ambartzumian, G. S. Sukiasian, G. K. Savvidy, and K. G. Savvidy, *Phys. Lett. B* **275**:99 (1992).
14. E. N. M. Cirillo, G. Gonnella, D. A. Johnston, and A. Pelizzola, *Phys. Lett. A* **226**:59 (1997).
15. M. E. Fisher and B. Widom, *J. Chem. Phys.* **50**:3756 (1968).
16. See, e. g., Gompper and M. Schick, Self-assembling Amphiphilic Systems, in *Phase Transitions and Critical Phenomena*, C. Domb and J. L. Lebowitz, eds. (Academic, London, 1994).
17. J. L. Moran-Lopez, F. Aguilera-Granja, and J. M. Sanchez, *J. Phys. Condense Matter* **6**:9759 (1994).
18. C. Buzano and M. Pretti, *Phys. Revs B* **56**:636 (1997).
19. B. Widom, *J. Chem. Phys.* **90**:2437 (1989).
20. J. Stephenson, J. Math. Phys. **11**:420 (1970); *Phys. Rev. B* **1**:4405 (1970).
21. I. Peschel and F. Rys, *Phys. Lett. A* **91**:187 (1982).
22. I. G. Enting, *J. Phys. C: Solid State Phys.* **10**:1379 (1977).